Multifractal comparison of the outputs of two optical disdrometers

Auguste Gires, Ioulia Tchiguirinskaia, D Schertzer

Multifractal comparison of the outputs of two optical disdrometers

Authors:

Gires A, Tchiguirinskaia I., Schertzer D.

Université Paris Est, Ecole des Ponts ParisTech, LEESU, Marne-la-Vallée, France

Abstract:

In this paper a Universal Multifractals comparison of the outputs of two types of collocated optical disdrometers installed on the roof of the Ecole des Ponts ParisTech is performed. A Campbell Scientific PWS100 which analyses the light scattered by the hydrometeors and an OTT Parsivel^2 which analyses the portion of occluded light are deployed. Both devices provide the binned distribution of drops according to their size and velocity. Various fields are studied across scales: rain rate (R), liquid water content (ρ), polarimetric weather radars quantities such the horizontal reflectivity (Z_h) and the specific differential phase (K_{dp}), and DSD parameters such as the total drop concentration (N_t) and the mass-weighted diameter (D_m).

For both devices a good scaling is retrieved on the whole range of available scales (2h – 30s), except for the DSD parameters for which the scaling only holds down to few minutes. For R, the UM parameters are found equal to 1.5 and 0.2 for respectively α and C_1. Results are interpreted with the help of the classical $Z_h - R$ and $R - K_{dp}$ radar relations.

Key words: multifractals, disdrometer, radar

1) Introduction

Rainfall measurement with the help of disdrometers is rapidly developing for point measurements. The first ones were impact disdrometers (Joss and Waldvogel 1967), and now optical ones (Loffler-Mang and Joss 2000, Ellis et al. 2006, Battaglia et al. 2010, Frasson et al. 2011) are more commonly used for operational and research purposes. The great advantage of these devices with regards to more conventional rain gauges is that they do not measure only a rain rate (or rainfall depth) but information about size and fall velocity for all the hydrometeors passing through the sampling area whose size is few tens of cm^2. The Drop Size Distribution (DSD) can then be computed from this raw data. From the DSD it is possible to estimate numerous rain related fields such as the rain rate (R) or the liquid water content (ρ) or even quantities measured directly by polarimetric weather radars such as the horizontal reflectivity (Z_h) and the specific differential phase (K_{dp}) (Jaffrain and Berne 2012, Leinonen et al. 2012, Verrier et al. 2013). This widens a lot the range of applications for disdrometer data.

Numerous experiments have been carried out to compare the rain rate output of various types of collocated disdrometers along with rain gauges (Miriovsky et al. 2004, Krajewski et al. 2006, Frasson et al., 2011, Thurai et al. 2011). The temporal evolution (Thurai et al 2011) or spatial distribution (Jaffrain and Berne 2011) of total drop concentration (N_t) and mass-weighted diameter (D_m), which are commonly used to fully characterize drop size distribution, have also been analysed. However these comparisons are usually done only at a single resolution, most commonly the maximum one available (i.e. using the time series at the recording time step). In this paper we suggest to carry out the comparison not only at a single scale but across scales. Considering various scales at once enables to obtained results robust over a wide range of scales. To achieve this, a theoretical framework relying on scale invariant properties is implemented. Available data enables to carry out analysis on scales

ranging from 30 s to approximately 2 hours for a punctual measure. Moreover not only R, ρ, or N_t and D_m, but also the radar quantities Z_h and K_{dp} will be investigated. The output data of two disdrometers, which have been deployed for few months on the roof of the Ecole des Ponts ParisTech building, will be used for this study. The two disdrometers are a Campbell Scientific PWS100 (Ellis et al. 2006, Campbell Scientific Ltd 2012), which has seldom been used in such study, and an OTT Parsivel^2 (Battaglia et al. 2010, OTT 2014).

The variability across scales will be quantified with the help of stochastic universal multifractals which have been extensively used to analyze, model, and simulate geophysical fields extremely variable over wide range of scales such as rainfall (Schertzer and Lovejoy 1987, 1997, Marsan et al. 1996, Olsson and Niemczynowicz 1996, Harris et al. 1997, de Lima and Grasman 1999, Lovejoy and Schertzer 2007, Nykanen 2008, Royer et al. 2008, de Lima and de Lima 2009, Mandapaka et al. 2009, de Montera et al. 2009, Verrier et al. 2010). This framework has seldom been applied to Z_h (see Tessier et al. 1993 for an example in space and not in time as here), and not to K_{dp} to the knowledge of the authors.

Data and the retrieval of the various studied fields are presented in section 2 along with a brief reminder of the Universal Multifractals (UM) framework and a presentation of the methodology implemented. Results are in section 4 where classical $Z_h - R$ of $R - K_{dp}$ relations are investigated with this data set, and scaling features and UM parameters estimates of the various fields are discussed.

2) Data and methods

2.1) Description of the disdrometer data

The data used in this paper was collected between 27 September 2013 and 18 January 2014 by two disdrometers installed on the roof of the Ecole des Ponts ParisTech building. They are both made of a transmitter that generates one or several laser sheet(s) and

receiver(s). The Campbell Scientific PWS100 computes size and fall velocity from light refracted by the hydrometeors (Ellis et al. 2006, Campbell Scientific Ltd 2012) whereas the OTT Parsivel^2 relies on occluded light (Loffler-Mang and Joss 2000, for an initial version; Battaglia et al. 2010, OTT 2014). The 50 recorded events of this period are used in this study. The criteria defining an event is a rainy period during which more than 1 mm is collected and that is separated by more than 15 min of dry conditions before and after. The main output of the disdrometers is a matrix with the number n_{ij} of drop recorded according to classes of equivolumic diameter (index i, and defined by a centre D_i and a width ΔD_i expressed in mm) and terminal fall velocity (index j, and defined by a centre v_j and a width Δv_j expressed in m.s^{-1}). This matrix is recorded for each 30s time step (Δt). Gires et al. (2014) which used the same data set noticed that the oblateness of drop was not properly taken into account in the PWS100 rationale and suggested a correction which is used here. Furthermore, as suggested by various authors (Jaffrain and Berne 2011, Kruger and Krajewski 2002, Thurai and Bringi, 2005) all the drops whose velocity was more than 60% different from what was expected by Beard's model (Beard 1977) according to its size were removed because considered as non meteorological measurements.

The rain rate for each time step is then computed as:

$$R_{PWS/Pars} = \frac{\pi}{6\Delta t}\sum_{i,j}\frac{n_{i,j}D_{PWS/Pars,i}^{3}}{S_{eff}(D_i)} \qquad (1)$$

where $S_{eff}(D_i)$ is the sampling area of the device which is slightly modified according to the drop size to take into account potential edge effects for large drops. For the Parsivel^2 we have $S_{eff}(D_i) = L\left(W - \frac{D_i}{2}\right)$, where L = 180 mm and W = 30 mm are respectively the length and width of the sensing area (LW = 54 cm^2) (OTT 2014). The PWS100 is not

99subject to this issue and S_{eff} is taken as constant equal to 40 cm^2 (Campbell Scientific Ltd
1002012). For the selected events the total rainfall depth collected is equal to 172 mm for the
101PWS100 and 154 mm for the Parsivel^2. A tipping bucket rain gauge is also located on the
102same roof and collected roughly 170 mm which is more in agreement with the PWS100, but it
103should not be “over-interpreted” given that its accuracy is not very high due to high rain rates
104and low level of maintenance at the beginning of the recording period. The normalized bias
105between the two disdrometers (computed for the time steps where R > 1mm/h) is equal to
1060.11; the correlation equals 0.96; the Nash-Sutcliffe efficiency coefficient equals 0.89 and the
107RMSE is 1.83. Although not negligible the differences between the two disdrometers are
108rather low compared to what is commonly observed (Miriovsky et al. 2004, Krajewski et al.
1092006, Frasson et al., 2011, Thurai et al. 2011).

110 A discrete drop size distribution (DSD) is computed from the available data as:

111 $$N(D_i) = \frac{1}{S_{eff}(D_i)\Delta D_i \Delta t}\sum_j \frac{n_{i,j}}{v_j} \quad (2)$$

112The number of drops with a diameter in the class i per unit volume (in m^{-3}) is given by
113$N(D_i)\ \Delta\ D_i$. As it is commonly done, we use the total drop concentration N_t (m^{-3}) and mass-
114weighted diameter D_m (mm) to characterize the DSD. In this framework the DSD is written as
115 $N(D) = N_t\, f(D_m)$; where it appears that D_m characterizes the shape of the DSD and N_t its
116total intensity. These two parameters are defined as (Jaffrain and Berne 2012a, Leinonen et al.
1172012):

118 $$N_t = \int_{D_{\min}}^{D_{\max}} N(D)dD \quad (3)$$

119 $$D_m = \frac{\int_{D_{\min}}^{D_{\max}} N(D)D^4 dD}{\int_{D_{\min}}^{D_{\max}} N(D)D^3 dD} \quad (4)$$

For the practical computation of these quantities (and the other ones), the integral is replaced by a summation over all the classes of diameter, i.e.:

$$\int_{D_{\min}}^{D_{\max}} f(D)N(D)dD \approx \sum_i f(D_i)N(D_i)\Delta D_i \qquad (5)$$

Lastly the liquid water content (ρ in g.m^{-3}) the horizontal reflectivity (Z_h in mm^6.m^{-3}) and the specific differential phase (K_{dp} in °.km^{-1}) are estimated with the help of the DSD from which they are basically various moments. These physical parameters are given by Jaffrain and Berne (2012a) and Leinonen et al. (2012):

$$\rho_l = \rho_w \frac{1}{10^3}\frac{4}{3}\pi\int_{D_{\min}}^{D_{\max}} N(D)\left(\frac{D}{2}\right)^3 dD \qquad (6)$$

With ρ_w,the liquid water density in g.m^{-3},

$$Z_{h,v} = \frac{\lambda^4}{\pi^5\left|\frac{m^2-1}{m^2+1}\right|}\int_{D_{\min}}^{D_{\max}} N(D)\sigma_{B;h}(D)dD \qquad (7)$$

$$K_{dp} = \frac{10^{-3}1800\lambda}{\pi}\int_{D_{\min}}^{D_{\max}} \mathrm{Re}\left[S_{hh}(D) - S_{vv}(D)\right]N(D)dD \qquad (8)$$

Where $\sigma_{B;h}$ (in mm^2) is the backscattering cross session at horizontal polarization, and Re($S_{hh/vv}$) (in mm) is the real part of the forward scattering amplitude at horizontal/vertical polarization, λ is the radar wavelength (in mm) and *m* the complex refractive index of water. The scattering coefficients were computed with the help of the Python PyTMatrix library (Leinonen 2014) which relies on the T-Matrix code by Mishchenko et al. (1996). Computations were carried out for a radar wave length equal to 53.5 mm corresponding to C-band radars (this wave length was chosen to facilitate comparison with other studies, because it is the most widely used and corresponds to the radar currently mostly used by Western European meteorological services), a temperature of 20°C (*m*=8.633 +1.289i) and an oblate spheroids model for drop shape with an axis ratio - equivolumic diameter relation corresponding to the one implemented in the Parsivel^2 rationale (Battaglia et al. 2010). The set

up considered for drop orientation was the same as in Leinonen (2012); i.e. drops are partially aligned and a normal distribution (mean and standard deviation respectively equal to 0° and 47°, in agreement with the findings of Bringi et al. 2008) characterizes the angle of the symmetry axis.

2.2) Methodology: UM framework

The key elements of the theoretical framework of UM are presented here and the reader is invited to refer to Schetzer and Lovejoy (2011) for a recent review. In the following ε_λ denotes a conservative field at resolution λ, defined as the ratio between the observation scale l and the outer scale L ($\lambda=L/l$). Practically ε_λ is obtained simply by up-scaling (averaging consecutive time steps) the measured field at the maximum resolution. If ε_λ is a multifractal field, then its statistical moment orders scale with resolution as:

$$\left\langle \varepsilon_\lambda{}^q \right\rangle \approx \lambda^{K(q)} \quad (9)$$

Where $K(q)$ is the moment scaling function that fully characterizes the variability across scales of the field ε_λ. The quality of the scaling is investigated with the help of the Trace Moment (TM) analysis which simply consists in plotting equation 9 in log-log, the slope of the obtained straight line being $K(q)$.

Most multiplicative processes converge toward Universal Multifractal which are fully characterized with the help of only two scale invariant parameters C_1 and α (this a broad generalization of the central limit theorem, Schertzer and Lovejoy 1987, 1997). C_1 is the mean intermittency co-dimension and measures the clustering of the (average) intensity at smaller and smaller scales (C_1=0 for a homogeneous field). α is the multifractality

index ($0 \leq \alpha \leq 2$) and measures the clustering variability with regards to intensity level. In this specific framework which is implemented here $K(q)$ is given by:

$$K(q) = \frac{C_1}{\alpha - 1}\left(q^{\alpha} - q\right) \quad (10)$$

The UM parameter are estimated in this paper with the help of the Double Trace Moment (DTM) technique (Lavallée et al. 1993).

A common framework to deal with a non-conservative field ϕ_λ (i.e. we have $\langle \phi_\lambda \rangle \neq 1$) is to assume it can written as

$$\phi_\lambda = \varepsilon_\lambda \, \lambda^{-H} \quad (11)$$

where H is the non-conservation parameter (H=0 for conservative fields), and ε_λ a conservative field characterized by a moment scaling function $K_c(q)$ depending only on UM parameters C_1 and α. More physically, this non-conservativeness means that the studied field ϕ_λ (the observations here) exhibits stronger correlations than the ones obtained with the help of a simple multifractal cascade and an additional fractional integration is needed to represent it. The moment scaling function $K(q)$ of ϕ_λ is given by:

$$K(q) = K_c(q) - Hq \quad (12)$$

H can be estimated with the help of (Tessier et al. 1993):

$$\beta = 1 + 2H - K_c(2) \quad (13)$$

where β is the spectral slope. It is the exponent of the power law that characterizes over large range of wave numbers the power spectrum of a scaling field:

$$E(k) \propto k^{-\beta} \quad (14)$$

Before going on let us clarify the relations between the notions of stationarity and conservation. For stochastic processes, stationarity refers to the fact that given statistics are

invariant with respect to time translations. When no given statistics are mentioned, it usually corresponds to the strongest case of stationarity, i.e. the probability itself is time translation invariant and therefore all the statistical moments are stationnary The classical case of "second order stationarity" is presumably the most cited case and is particularly important for additive processes. It corresponds to time translation invariance of the second order moments of the increments. For multiplicative processes, conservation means that a given statistic is strictly independent from scale, in general this statistic is the mean of the field (H=0 in Eq. 11). The latter implies a given form of stationarity because at all scales the fluctuations remain around this mean. However, these fluctuations are not only easily wilder than for an additive process, but their amplitude generally increases with smaller and smaller scales. Conversely, non-conservation implies a strong non stationarity, starting with the fact that the mean has a scaling behaviour (Eq. 11). For instance, a spectral analysis will detect the non conservation ($H \neq 0$), due to the departure of the spectral slope, which is a second order statistic, from that of "a pink noise" (k^{-1}), where the exponent one corresponds here to the dimension of the embedding space (time series are studied here). With multifractal fields there is a further correction with the $K_c(2)$ (Eq. 13) which is not negligible (in the range 0.1-0.4 for the retrieved UM parameters).

The TM and DTM techniques are designed for analysing conservative fields (H=0) and remain reliable as long as H<0.5. In case of greater H, they should be implemented not on ϕ_λ, but on the underlying conservative field ε_λ. A fractional integration of order H (equivalent to a multiplication by k^H in the Fourier space) is theoretically required to estimate ε_λ from ϕ_λ. However a common approximation (Lavallée et al. 1993) which provides reliable results consists in taking ε_Λ at the maximum resolution simply equal to the renormalized absolute value of the fluctuations of the field i.e.:

$$\varepsilon_\lambda = \frac{|\phi_\lambda(i+1) - \phi_\lambda(i)|}{\langle |\phi_\lambda(i+1) - \phi_\lambda(i)| \rangle} \qquad (15)$$

and then upscaling this field at other resolutions λ.

Spectral and multifractal analyses are implemented on ensemble average over various samples, i.e. each sample is considered as a realization of the process. For example it means that each sample is up-scaled and taken to the power *q* independently before taking the average in equation 9. The studied samples are extracted in the following way from the selected events: for each event (i) a sample size is chosen (necessarily a power of two); (ii) the maximum number of samples for this event is computed; (iii) the portion of the event of length equal to the sample size multiplied by the number of samples found in (ii) with the greatest cumulative depth is extracted; (iv) the extracted series is cut into various samples.

Given that the sample size is a power of two there is obviously some data lost during the selection process. Here the percentage of available data actually used is equal to 36, 65, 82 and 91% for samples of size 512, 256, 128 and 64 times steps of 30s respectively. The chosen sample size should result from a trade off between the width of the available range of scales which should be as great as possible, and the amount of wasted data which reduces the reliability of the estimates. Here we chose to analyse the scaling properties with samples of size 256 (approximately 2h, 46 samples available), and given that no scaling break was identified on the main studied fields, UM parameters were estimated with samples of size of 64 (approximately 30 min, 259 samples available) to benefit from the use of more data. Finally it should be mentioned that since D_m is not defined when there are no drops, only the samples containing drops at all time steps are used for this field.

3) Results and discussion

3.1) Standard radar relationships

Given that it was possible to retrieve both rain rates and radar parameters, it is possible to analyse the validity, for this data set, of the standard power law relations that are commonly assumed between these quantities:

$$Z_h = aR^b \quad (16)$$

$$R = cK_{dp}^{\ d} \quad (17)$$

These relations will be used in the following sections to help in the interpretation of the observed scaling features exhibited by each quantity. Various authors (Campos and Zawadzki 2000, Jaffrain and Berne 2012b, Verrier et al. 2013) noticed a strong sensitivity of the estimates of *a* and *b* on the method implemented to compute them. Here we performed an orthogonal linear regression, which does not assume any dependent variable, on the logs of Z_h, R and K_{dp}. The regressions are performed only for the time steps for which $K_{dp} > 10^{-2}$ because we noticed that small values in which we are not interested had a strong influence on the retrieved parameters. Figures 1.a and 1.b display the regressions for the two relations and both devices, and the retrieved values for *a*, *b*, *c* and *d* are shown in Table 1. It appears that the quality of the fitting is comparable for the two relationships and slightly better for the PWS100 than for the Parsivel^2 ($r^2 \sim 0.8$ vs. 0.75). The estimates are similar for both devices. More precisely for the $Z_h - R$ relation *a* is slightly greater and *b* slightly smaller for the PWS100 that for the Parsivel^2, meaning that the effects of each other are compensating. For the $R - K_{dp}$ relationship *c* and *d* are both slightly greater for the PWS100, meaning a given value of K_{dp} will systematically yield greater estimates of R with the PWS100 values. The estimates of the exponents are in the range of those commonly observed (Jaffrain and Berne 2012b, Figuras I ventura et al. 2013, Verrier et al. 2013). With regards to *a* values they are in agreement with those found by Verrier et al. (2013), and in the upper range of those reported by Jaffrain and Berne (2012b). The *c* values are similar to those found by Jaffrain and Berne (2012b). Relations 16 and 17 are studied only at the maximum resolution (30 s) and the strong

scale dependency of the parameters *a*, *b*, *c* and *d* is not investigated here (see Verrier et al. 2013 for an analysis of this issue for $Z_h - R$ relation). Parameters are computed here taking into account all the events at once, meaning that "climatic" (keeping in mind only 4 months of data are used) estimates are studied. An event based analysis will be discussed in future works. It is indeed not needed for the purpose of this paper, which is to quantify the scaling variability observed by the two disdrometers on various fields.

Finally the influence of using the retrieved "climatic" parameters for computing rain rates from radar parameters is assessed. With this purpose, the rain rates computed either directly from raw data (R) or through the radar relations 16 and 17 (respectively R_{Z-R} and $R_{R-K_{dp}}$) once Z_h and K_{dp} have been estimated with raw data are compared. Figure 1.c and 1.d display, for the PWS100 data, a scatter plot for the $Z_h - R$ and $R - K_{dp}$ relations respectively. Similar curves are obtained for the Parsivel[2] data and not shown here. The scattering around the bisector is not negligible with a 30 s time step, and is more pronounced for the $Z_h - R$ than for the $R - K_{dp}$ relation which means that the use of "climatic" values is less acceptable for the former. It should also be noted that there is a tendency of underestimating large rain rate with the $R - K_{dp}$ relation, indeed $R_{R-K_{dp}}$ is systematically smaller than R for R>50 mm/h. The total rainfall depths between the three techniques are very similar with roughly 3% or less differences.

3.2) Scaling behaviour

The scaling features of the various fields are studied in this section. Figure 2.a displays the spectral analysis (i.e. equation 14 in log-log plot) of the rain rate for the PWS100. A very good scaling (i.e. a straight line) is observed on the whole range of available scales (30s – 2h).

The spectral slope is greater than the embedding dimension of the field (1 for time series) suggesting that R is non-conservative (this will be confirmed in the next session with the estimation of H). A practical consequence is that the TM analysis which assumes a conservative field should not be implemented on the field itself but only on its conservative part which can the approximated by the absolute value of its fluctuations (equation 15). The results are displayed on Fig. 2.b, where the good scaling with a unique regime is confirmed. The r^2 for q = 1.5 which is taken as an indication of the quality of the scaling is greater than 0.99. The same analysis carried out directly on the field yields non aligned points with a flattening for small scales (r^2 = 0.94 for q = 1.5). Same curves for spectral and TM analyses for the Parsivel^2 data are shown in Fig. 2.c and 2.d respectively. It appears that very similar results are found for the Parsivel^2 data. Similar curves for both devices are also obtained for the other studied quantity (ρ, K_{dp}, Z_h, N_t, D_m), therefore in the following only the curves for PWS100 will be showed and discussed in this sub-section.

Very similar results are found for ρ and K_{dp} (Fig. 3) with a very good scaling on the whole range of available scales on both the spectra and the TM analysis, which also has to be conducted on the fluctuations of the field. The good scaling behaviour retrieved for K_{dp} is not surprising and was actually expected if relation 17 is correct. Indeed a power (K_{dp} here) of a multifractal field (R here) should also behave as a multifractal field (this is the basic concept behind the DTM technique). To the knowledge of the authors, the multifractal behaviour of K_{dp} has not yet been studied in time with disdrometer data this way, and it opens new perspectives. A potential one would be to compare these outputs with similar analysis performed in space with data provided by weather data. This would enable to study scaling relations in a spatio-temporal framework with a quantity directly measured by the radar (so far the only device providing “rather” high resolution space-time data of rain related fields)

without having to rely on tailored relations that may introduce biases in the scaling behaviour as it is the case for the rain rate.

The situation for Z_h is more complex. Indeed the energy spectrum (Fig. 4.a) is not linear and could be interpreted as exhibiting two breaks, one at roughly 6 min^{-1} and the other one (the minimum on the curve) at roughly 2 min^{-1}. Authors do not have explanation for this behaviour which is not retrieved on R and K_{dp}. It was not expected and suggests that the "climatic" relation 16 does not hold very well. Indeed if it was true, a good scaling behaviour would be observed on the spectra. To confirm this, the same analysis were carried out on the quantity aR^b, where R is the rain rate studied before and a and b are the "climatic" values estimated in section 3.1. As expected for this analysis a good scaling behaviour is indeed retrieved on both the spectra (Fig. 4.c) and the TM analysis (Fig. 4.d). It should be mentioned that the greater scattering of the points for the $Z_h - R$ than the $R - K_{dp}$ relation observed on Fig. 1 is consistent with the fact that we found a good scaling behaviour on R and K_{dp} and not Z_h. Quite surprisingly the scaling breaks observed on the spectra are not visible on the TM analysis (Fig. 4.b) where a unique regime is observed. It was implemented on the fluctuations of the field (Eq. 15) for which there are a slightly better scaling than for the field itself. However given the lack of scaling observed in the spectral analysis, the TM analysis might be not very reliable and should not be over-interpreted.

Finally we analysed the scaling features of N_t and D_m which are used to characterize the shape of the DSD. For N_t we find a good spectral behaviour but limited to the range 2 min – 2 h, as a flattening of the spectra is observed for small scales (Fig. 5.a). Similarly to the previously studied fields, a spectral slope greater that one is found meaning that the TM analysis should not be performed on the field directly but on its fluctuations (equation 15). It is displayed in Fig. 5.b and it appears that a good scaling behaviour is retrieved on a range of scales (4 min – 2 h) similar to the one observed on the spectra (Fig. 5.a). Considering the

whole range of scales would lead to a r^2 for q = 1.5 equal to 0.96 whereas is of 0.99 on the limited range of scales. Similar scaling regimes are observed on D_m's spectra (Fig. 6.a), but the slope is much lower meaning that the TM analysis should be conducted directly on the field. It yields a good scaling behaviour with a r^2 for q = 1.5 equal to 0.99 (it is of 0.87 if the TM analysis is conducted on the fluctuations) (Fig. 6.b). The flattening of the spectra (almost a horizontal slope) for small scales corresponds to what would be observed for a white noise. This would suggest that N_t and D_m exhibit a scaling structure down to few minutes and behave as a random homogeneous variable for smaller scales. It is not possible to confirm this interpretation with the help of this data. More data at higher resolution, which would extend the range of available small scales, would be needed to achieve this. A possible interpretation of this could simply be that the sampling uncertainty is more visible at smaller scales and for these quantities than the other ones.

3.3) UM parameters

Estimates of UM parameters for the various studied fields and the two devices are reported in Table 2. It is timely to mention that the proportion of zeros is quite low (12 %, with a fractal dimension of 0.96), which means that estimates are not biased by the multifractal phase transition for small moment orders which is associated with them (see Gires et al., 2012 for a in-depth analysis of this effect). Given the low quality of the scaling in the spectral analysis for Z_h, the values of β and H are not shown for this field since they are not reliable.

For all the fields we find H values greater than 0.5, except for D_m, which confirms that the studied fields are non-conservative, and that the UM parameters α and C_1 should indeed be estimated on their fluctuations as it was done. The estimates of the characteristic scaling

parameters are very similar for the two devices. It means that despites a roughly 10% difference in terms of rain rate; they both record the same variability across scales. The estimates for the rain rate, which is the field that has been mostly studied, are comparable with the ones usually found for this range of scales by authors focusing the analysis on the rainy portions (de Montera et al. 2009, Mandapaka et al. 2009, Verrier et al. 2010, Gires et al. 2013), although with slightly smaller values of α which were commonly reported to 1.8. With regards to D_m and Z_h the differences between the two devices are more pronounced but it is harder to interpret this fact given that the lower quality of the scaling for these fields implies less reliable estimates.

It is possible to give an insight into radar relations 16 and 17 through the UM parameters estimates. Indeed if a field is multifracal, then as previously mentioned a power of it is also multiractal, and there is furthermore a relation between the α and C_1 (Tessier et al. 1993, Lovejoy et al. 2008) More precisely, if $R = cK_{dp}^{\ d}$, we have:

$$\alpha_R = \alpha_{K_{dp}} \qquad (18.a)$$

$$C_{1,R} = d^{\alpha} C_{1,K_{dp}} \qquad (18.b)$$

Here for both devices we find a roughly 0.2 difference between α computed for the two fields. With regards to C_1, for the PWS100 data $C_{1,R} / d_{PWS}^{\ \alpha_R} = 0.29$ (the value is slightly smaller when considering $\alpha_{K_{dp}}$ in the relation) which is in rather good agreement with the 0.23 retrieved on the K_{dp} field. For the Parsivel[2] data $C_{1,R} / d_{Pars}^{\ \alpha} = 0.35$ which yields a value greater than the 0.25 retrieved on the K_{dp} field. The same computations can be carried out for the $Z_h - R$ relation. Indeed if $Z_h = aR^b$, one expects:

$$\alpha_{Z_h} = \alpha_R \qquad (19.a)$$

$C_{1,Z_h} = b^{\alpha} C_{1,R}$ (19.b)

The difficulty here is that the agreement between the estimates of α is worse than for the $R - K_{dp}$ relation and the scaling on Z_h is not very good and reliable. With regards to C_1 we have $b_{PWS}^{\alpha_{PWS,R}} C_{1,R_{PWS}} = 0.32$ (a slightly greater value is found using α_{Z_h}) which is quite close to 0.34 found on Z_h, and $b_{Pars}^{\alpha_{Pars,R}} C_{1,R_{Pars}} = 0.39$ (a slightly greater value is found using α_{Z_h}) which is quite different from the 0.51 found on Z_h. Finally it should be mentioned that the estimates of α and C_1 on the field $a_{PWS} R_{PWS}^{b_{PWS}}$ (see Fig. 4.c and 4.d for scaling curves) are respectively 1.55 and 0.28 which is roughly in agreement with equation 19 ($b_{PWS}^{\alpha_{PWS}} C_{1,R_{PWS}} = 0.32$). The differences noticed with regards to the underlying theoretical framework highlight the limitation of the "climatic" relations 16 and 17. The better agreement in equations 18 and 19 for the PWS100 data is consistent with the greater quality of the fitting of relations 16 and 17 for the PWS100 than for the Parsivel[2] (Fig. 1). The fact the α are equal for R, ρ and N_t also suggests that a power-law relation between these quantities could be investigated, which is not surprising since these quantities correspond to various moments of the DSD (Sempere-Torres et al. 2000, Lee et al. 2004, Lovejoy and Schertzer 2008, Verrier et al. 2013), even more directly than Z_h and K_{dp}, but this is beyond the scope of this paper.

4) Conclusions

In this paper the output data provided by two optical disdrometers is analysed; the Campbell Scientific PWS100 based on the analysis of the light refracted by drops and the

401OTT Parsivel^2 based on the analysis of light occluded by drops. Not only the rainfall rate, but
402also the DSD parameters N_t and D_m, and the radar parameters Z_h and K_{dp} are studied.
403Furthermore the analysis is not performed only at the maximum resolution as it is commonly
404done but across scales with the help of the theoretical framework of Universal Multifractals.
405 It appears that despite a roughly 10 % differences in terms of rain rate, the multifractal
406analysis yield very similar results for the two measuring devices, with a slightly worse scaling
407observed on the Parsivel^2 data. R exhibits a very good scaling on the whole range of available
408scales (30 s – 2h) with H=0.7, C_1=0.2 and α=1.5 which confirms findings of previous studies.
409A very good scaling is also retrieve on K_{dp} and UM parameters estimates are in rather good
410agreement with what would be expected if the standard relation $R = cK_{dp}^{\ d}$ is implemented
411with "climatic" parameters computed for this data set. The scaling of Z_h is worse, especially
412on the spectra, which highlights some limitations of the power law relation $Z_h = aR^b$. Finally
413the scaling behaviour only holds on the range few min – 2 h for N_t and D_m, and there are some
414hints at a possible random uniform behaviour for smaller scales possibly associated with
415sampling uncertainty.
416 These results suggest new ways of comparing the outputs of disdrometers by using
417other fields than the rain rate, and also scaling analysis. The results are particularly promising
418for K_{dp} which is also directly measured by polarimetric weather radars, contrarily to the rain
419rate for which non-trivial transformations potentially biasing the observed scaling are
420implemented. Multifractal investigations in a spatio-temporal framework on K_{dp} radar data
421should be carried out to improve knowledge about rainfall as a space-time process. More data,
422including spatial ones, should be analysed to confirm the possibility of characterizing DSD
423parameters with the help of UM, and hence the possibility of developing coupled multifractal
424cascades to actually simulate DSD fields.

Acknowledgments

Authors thanks Serge Botton (from the “Département Positionnement Terrestre et Spatial” of the ENSG) for facilitating access to the roof where the disdrometers are installed. Authors greatly acknowledge partial financial support form the Chair “Hydrology for Resilient Cities” (sponsored by Veolia) of Ecole des Ponts ParisTech, EU NEW INTERREG IV RainGain Project (www.raingain.eu), and EU Climate KIC Blue Green Dream (www.bgd.org.uk)

References:

Battaglia, A., Rustemeier, E., Tokay, A., Blahak, U. and Simmer, C., 2010. PARSIVEL Snow Observations: A Critical Assessment. *Journal of Atmospheric and Oceanic Technology*, 27(2), 333-344.

Beard, K.V., 1977. Terminal velocity adjustment for cloud and precipitation aloft. *J. Atmos. Sci*, 34, 1293-1298.

Bringi, V.N., Thurai, M. and Brunkow, D.A., 2008. Measurements and inferences of raindrop canting angles. *Electronics Letters*, 44(24), 1425-1426.

Campbell-Scientific-Ltd, 2012. PWS100 Present Weather Sensor, User Guide

Campos, E. and Zawadzki, I., 2000. Instrumental Uncertainties in Z-R Relations. *Journal of Applied Meteorology*, 39(7), 1088-1102.

de Lima, M.I.P. and de Lima, J., 2009. Investigating the multifractality of point precipitation in the Madeira archipelago. *Nonlinear Processes in Geophysics*, 16(2), 299-311.

de Lima, M.I.P. and Grasman, J., 1999. Multifractal analysis of 15-min and daily rainfall from a semi-arid region in Portugal. *Journal of Hydrology*, 220(1-2), 1-11.

de Montera, L., Barthes, L., Mallet, C. and Gole, P., 2009. The Effect of Rain-No Rain Intermittency on the Estimation of the Universal Multifractals Model Parameters. *Journal of Hydrometeorology*, 10(2), 493-506.

Ellis, R.A. et al., 2006. New laser technology to determine present weather parameters. *Measurement Science & Technology*, 17(7), 1715-1722.

Figueras i Ventura, J. and Tabary, P., 2013. The New French Operational Polarimetric Radar Rainfall Rate Product. *Journal of Applied Meteorology and Climatology*, 52(8), 1817-1835.

Frasson, R.P.d.M., da Cunha, L.K. and Krajewski, W.F., 2011. Assessment of the Thies optical disdrometer performance. *Atmospheric Research*, 101(1-2), 237-255.

Gires, A., Tchiguirinskaia, I., Schertzer, D. and Lovejoy, S., 2012. Influence of the zero-rainfall on the assessment of the multifractal parameters. *Advances in Water Resources*, 45, 13-25.

Gires, A., Tchiguirinskaia, I., Schertzer, D. and Lovejoy, S., 2013. Development and analysis of a simple model to represent the zero rainfall in a universal multifractal framework. *Nonlin. Processes Geophys.*, 20(3), 343-356.

Gires, A., Tchiguirinskaia, I., Schertzer, D., 2014. Improvement of measurement with a refraction disdrometer by better taking into account the drops oblateness, in preparation

Harris, D., Menabde, M., Seed, A. and Austin, G., 1997. Factors affecting multiscaling analysis of rainfall time series. *Nonlinear Processes in Geophysics*, 4, 137-155.

Jaffrain, J. and Berne, A., 2012a. Influence of the Subgrid Variability of the Raindrop Size Distribution on Radar Rainfall Estimators. *Journal of Applied Meteorology and Climatology*, 51(4), 780-785.

Jaffrain, J. and Berne, A., 2012b. Quantification of the Small-Scale Spatial Structure of the Raindrop Size Distribution from a Network of Disdrometers. *Journal of Applied Meteorology and Climatology*, 51(5), 941-953.

Joss, J. and Waldvogel, A., 1967. Ein spektrograph fur nieder chlagstropfen mit automatischer auswertung (A spectrograph for raindrops with automatic interpretation). *Pure Appl. Geophys. Rev. A.*, 68, 240-246.

Krajewski, W.F. et al., 2006. DEVEX-disdrometer evaluation experiment: Basic results and implications for hydrologic studies. *Advances in Water Resources*, 29(2), 311-325.

Kruger, A. and Krajewski, W.F., 2002. Two-Dimensional Video Disdrometer: A Description. *Journal of Atmospheric and Oceanic Technology*, 19(5), 602-617.

Lavallée, D., Lovejoy, S. and Ladoy, P., 1993. Nonlinear variability and landscape topography: analysis and simulation. In: L. de Cola and N. Lam (Editors), Fractas in geography. Prentice-Hall, pp. 171-205.

Lee, G.W., Zawadzki, I., Szyrmer, W., Sempere-Torres, D. and Uijlenhoet, R., 2004. A General Approach to Double-Moment Normalization of Drop Size Distributions. *Journal of Applied Meteorology*, 43(2), 264-281.

Leinonen, J., 2014. High-level interface to T-matrix scattering calculations: architecture, capabilities and limitations. *Optics Express*, 22(2), 1655-1660.

Leinonen, J., Moisseev, D., Leskinen, M. and Petersen, W.A., 2012. A Climatology of Disdrometer Measurements of Rainfall in Finland over Five Years with Implications for Global Radar Observations. *Journal of Applied Meteorology and Climatology*, 51(2), 392-404.

Loffler-Mang, M. and Joss, J., 2000. An Optical Disdrometer for Measuring Size and Velocity of Hydrometeors. *Journal of Atmospheric and Oceanic Technology*, 17(2), 130-139.

Lovejoy, S. and Schertzer, D., 2007. Scale, scaling and multifractals in geophysics: Twenty years on. *Nonlinear Dynamics in Geosciences*, 311-337 pp.

Lovejoy, S. and Schertzer, D., 2008a. Turbulence, rain drops and the l**1/2 number density law. *New J. of Physics*, 10, 32pp.

Lovejoy, S., Schertzer, D. and Allaire, V., 2008b. The remarkable wide range spatial scaling of TRMM precipitation. *J. Atmos. Research*, 90, 10-32.

Mandapaka, P.V., Lewandowski, P., Eichinger, W.E. and Krajewski, W.F., 2009. Multiscaling analysis of high resolution space-time lidar-rainfall. *Nonlinear Processes in Geophysics*, 16(5), 579-586.

Marsan, D., Schertzer, D. and Lovejoy, S., 1996. Causal space-time multifractal processes: Predictability and forecasting of rain fields. *J. Geophys. Res.*, 101, 26333-26346.

Miriovsky, B.J. et al., 2004. An Experimental Study of Small-Scale Variability of Radar Reflectivity Using Disdrometer Observations. *Journal of Applied Meteorology*, 43(1), 106-118.

Mishchenko, M.I., Travis, L.D. and Mackowski, D.W., 1996. T-matrix computations of light scattering by nonspherical particles: A review. *Journal of Quantitative Spectroscopy and Radiative Transfer*, 55(5), 535-575.

Nykanen, D.K., 2008. Linkages between Orographic Forcing and the Scaling Properties of Convective Rainfall in Mountainous Regions. *J. of hydrometeorology*, 9, 327-347.

Olsson, J. and Niemczynowicz, J., 1996. Multifractal analysis of daily spatial rainfall distributions. *J. of hydrology*, 187, 29-43.

OTT, 2014. Operating instructions, Present Weather Sensor OTT Parsivel2.

Schertzer, D. and Lovejoy, S., 1987. Physical modelling and analysis of rain and clouds by anisotropic scaling and multiplicative processes. *J. Geophys. Res.*, 92(D8), 9693-9714.

Schertzer, D. and Lovejoy, S., 1997. Universal multifractals do exist!: Comments. *Journal of Applied Meteorology*, 36(9), 1296-1303.

Schertzer, D. and Lovejoy, S., 2011. Multifractals, generalized scale invariance and complexity in geophysics. *International Journal of Bifurcation and Chaos*, 21(12), 3417-3456.

Sempere-Torresl, D., Sanchez-Diezma, R., Zawadzki, I. and Creutin, J.D., 2000. Identification of stratiform and convective areas using radar data with application to the improvement of DSD analysis and Z-R relations. *Physics and Chemistry of the Earth, Part B: Hydrology, Oceans and Atmosphere*, 25(10-12), 985-990.

Tessier, Y., Lovejoy, S. and Schertzer, D., 1993. Universal Multifractals: theory and observations for rain and clouds. *Journal of Applied Meteorology*, 32(2), 223-250.

Thurai, M. and Bringi, V.N., 2005. Drop Axis Ratios from a 2D Video Disdrometer. *Journal of Atmospheric and Oceanic Technology*, 22(7), 966-978.

Thurai, M., Peterson, W.A., Tokay, A., Schutz, C. and Gatlin, P., 2011. Drop size distribution comparisons between Parsivel and 2-D video disdrometers. *Advances in Geosciences*, 30, 3-9

Table:

		PWS100	Parsivel[2]
$Z_h - R$	a	349	313
	b	1.49	1.63
$R - K_{dp}$	c	17.3	15.3
	d	0.72	0.66

Table 1: Parameters computed for the $Z_h - R$ relation (Equation 16) and the $R - K_{dp}$ relation (Equation 17)

		R	ρ	K_{dp}	Z_h	N_t	D_m
PWS100	β	2.05	2.08	1.88	-	2.07	1.41
	α	1.51	1.53	1.35	1.72	1.58	1.66
	C_1	0.18	0.16	0.23	0.34	0.11	0.005
	H	0.67	0.67	0.62	-	0.63	0.21
Parsivel[2]	β	1.96	2.08	1.71	-	2.11	1.33
	α	1.57	1.54	1.33	2.00	1.60	2.10
	C_1	0.18	0.16	0.25	0.51	0.11	0.006
	H	0.63	0.67	0.55	-	0.64	0.17

545Table 2: Scaling parameters of the various studied fields for the PWS100 and Parsivel[2] data

546

547

548

549**Figure caption list:**

550

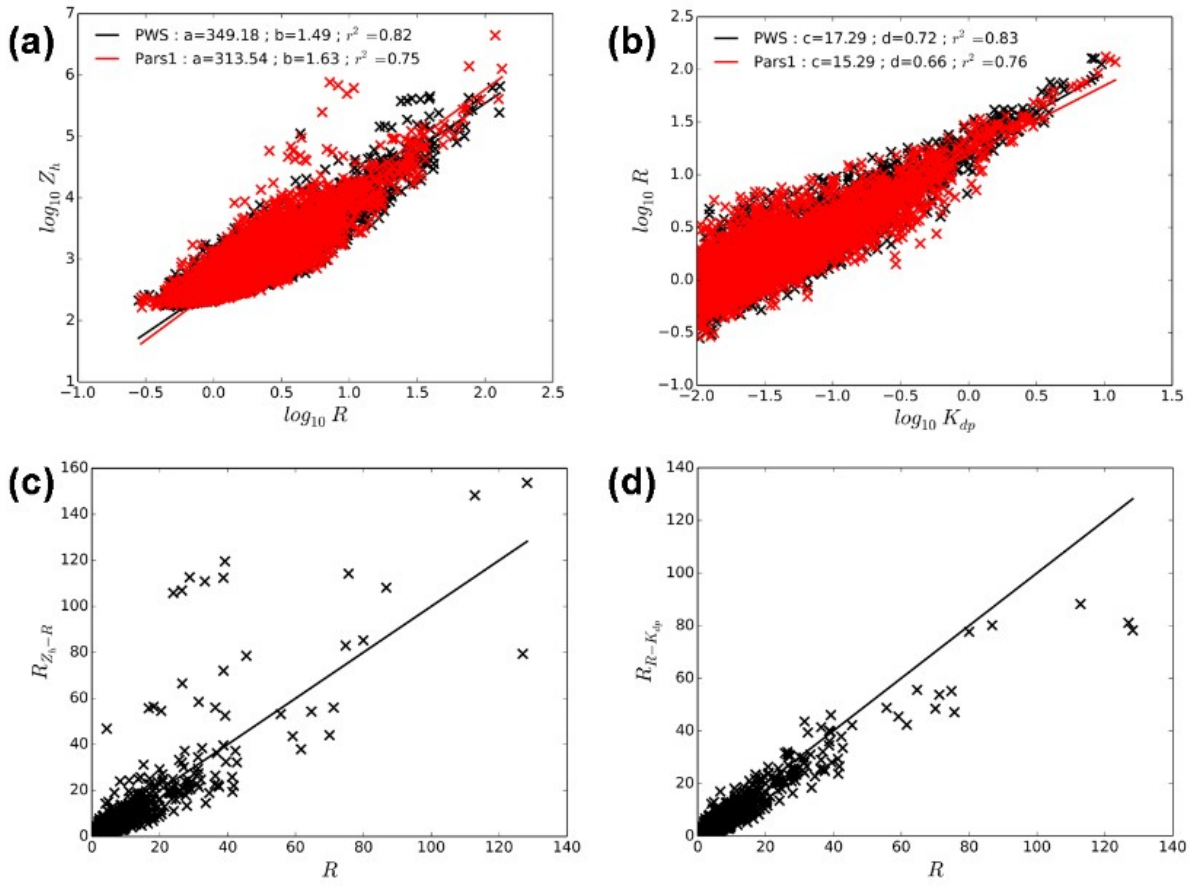

551

552Figure 1: Computation of the parameters of the $Z_h - R$ (a) and $R - K_{dp}$ (b) relations

553(equations 16 and 17 respectively in log-log plot). Scatter plot of R_{Z-R} (c) and $R_{R-K_{dp}}$ (d)

554versus *R* for the PWS100 data

555

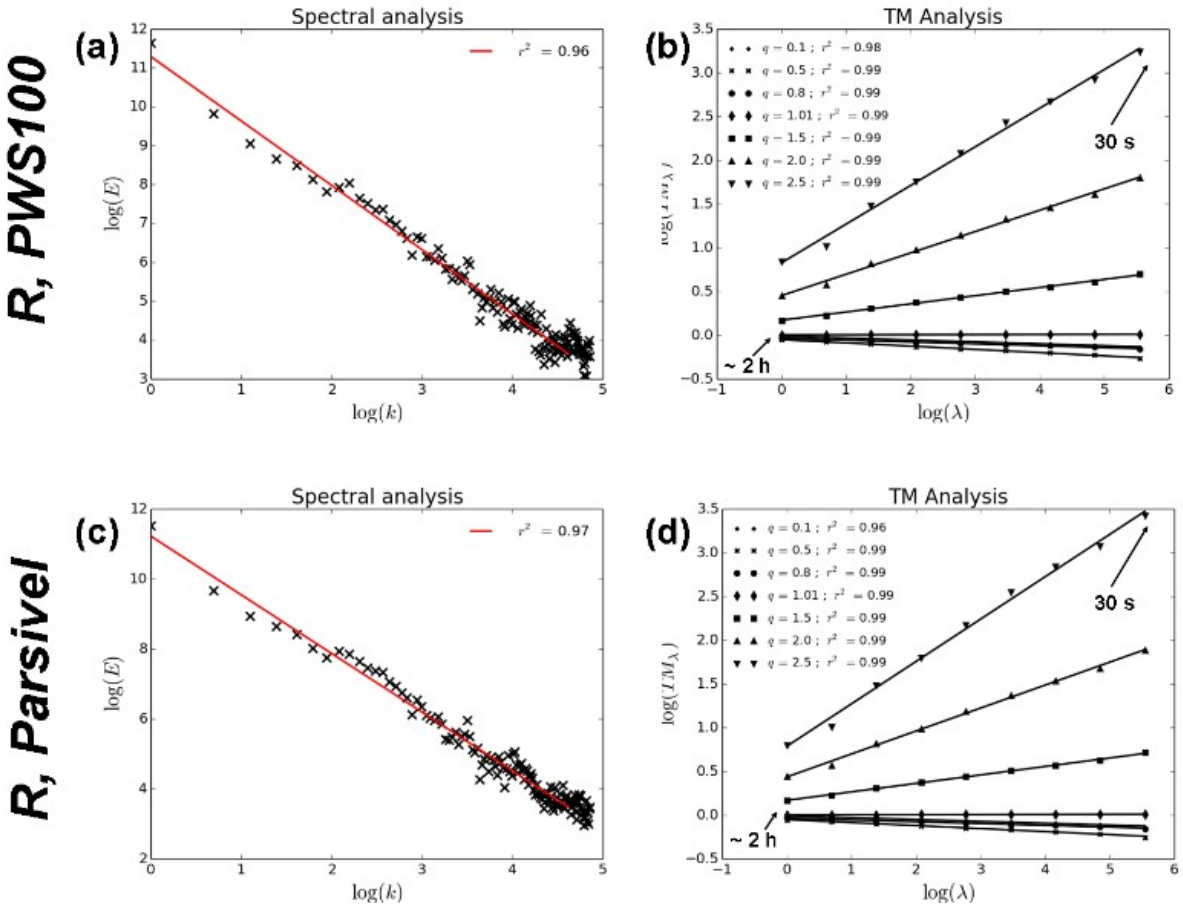

556

557Figure 2: Scaling analysis for *R* measured by the PWS100: (a) Spectral analysis, i.e. equation

55814 in log-log plot; (b) Trace Moment (TM) analysis, i.e. equation 9 in log-log plot. (c) and (d)

559Same as (a) and (b) for *R* measured by the Parsivel[2].

560

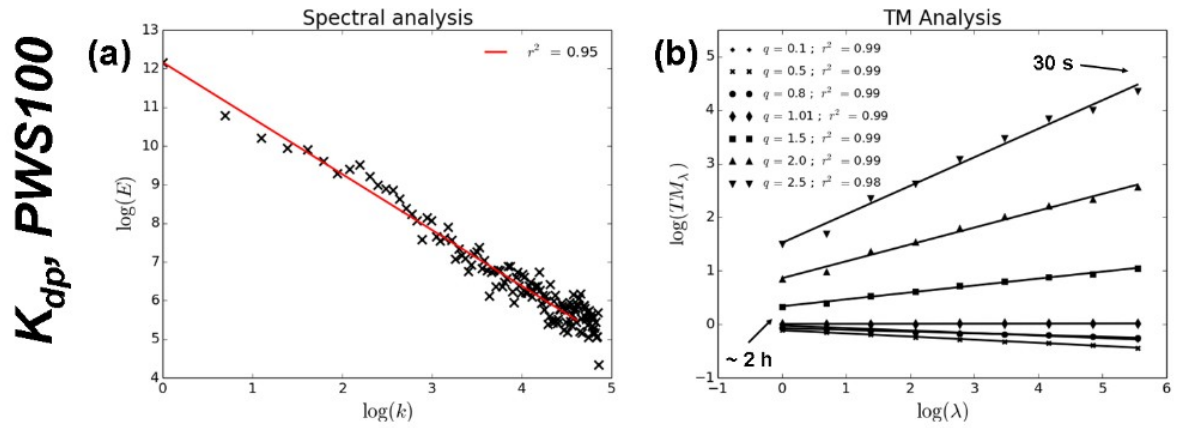

561

562Figure 3: Scaling analysis for K_{dp} measured by the PWS100: (a) Spectral analysis, i.e.

563equation 14 in log-log plot; (b) Trace Moment (TM) analysis, i.e. equation 9 in log-log plot

564

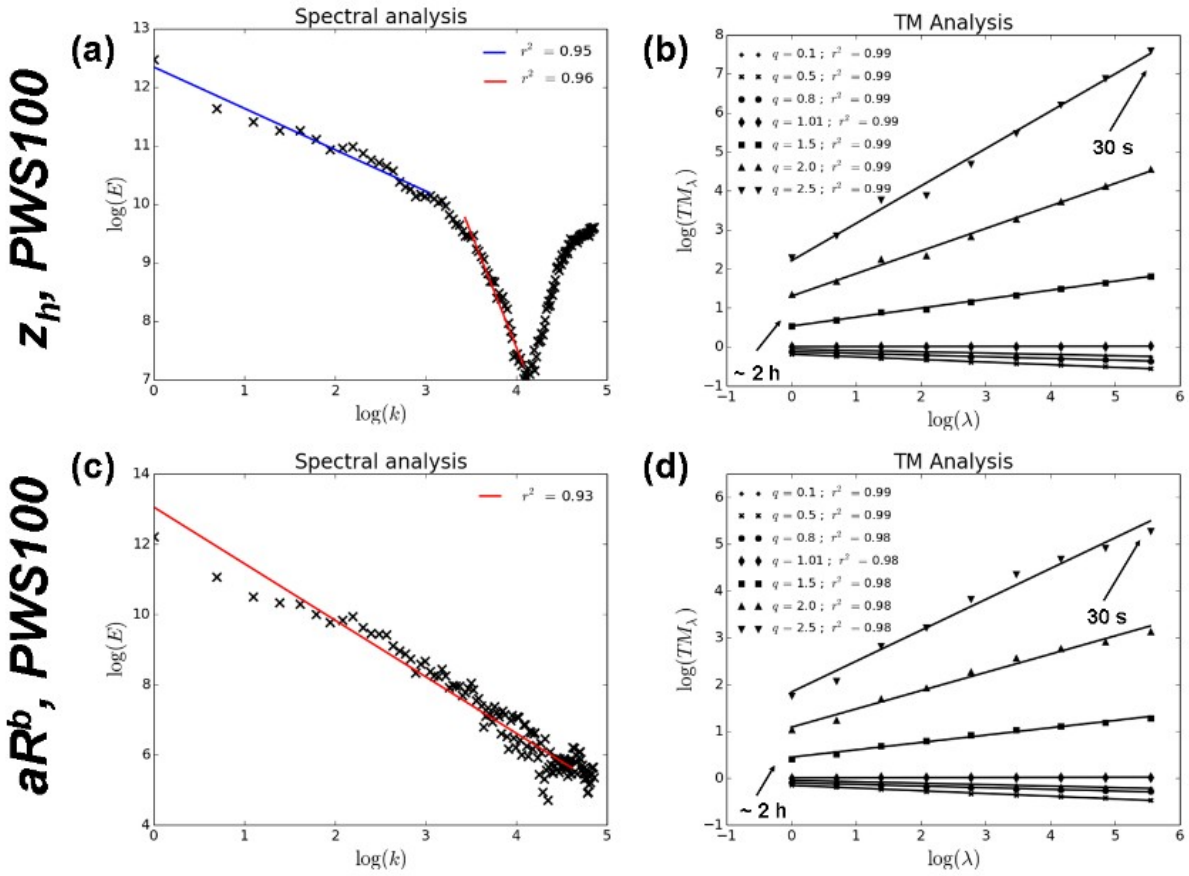

565

566Figure 4: (a) – (b) Same as in Fig. 3 but for Z_h measured by the PWS100, in (a) a break is

567considered for k = 20-30 (~ 6 min^{-1}) and k = 60 (~ 2 min^{-1}); (c) – (d) Same as in Fig. 3 but for

568 aR^b measured by the PWS100 and "climatic" parameters a and b found in section 2.

569

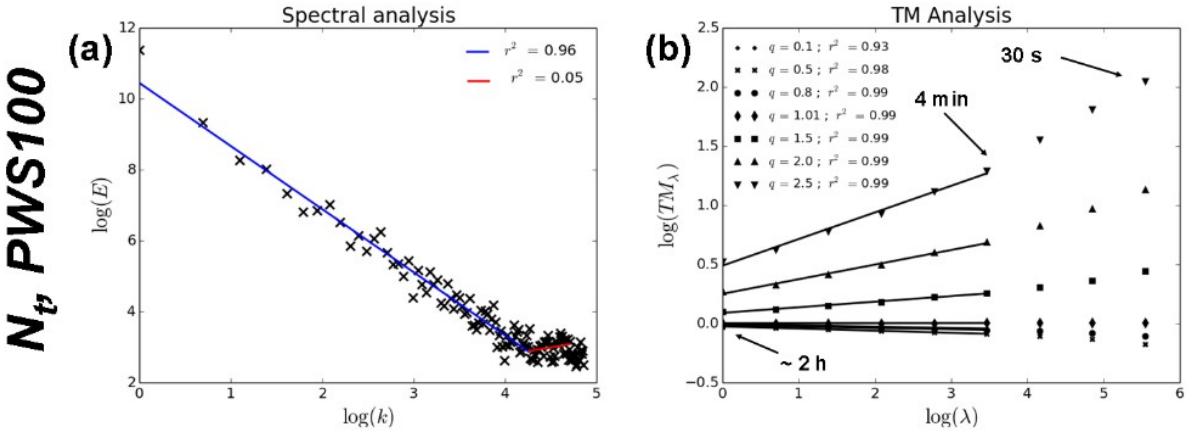

570

571Figure 5: Same as in Fig. 3 but for N_t measured by the PWS100, in (a) a break is considered

572for k=70 (~ 2 min^{-1}), in (b) a break is considered for λ=32 (4 min)

573

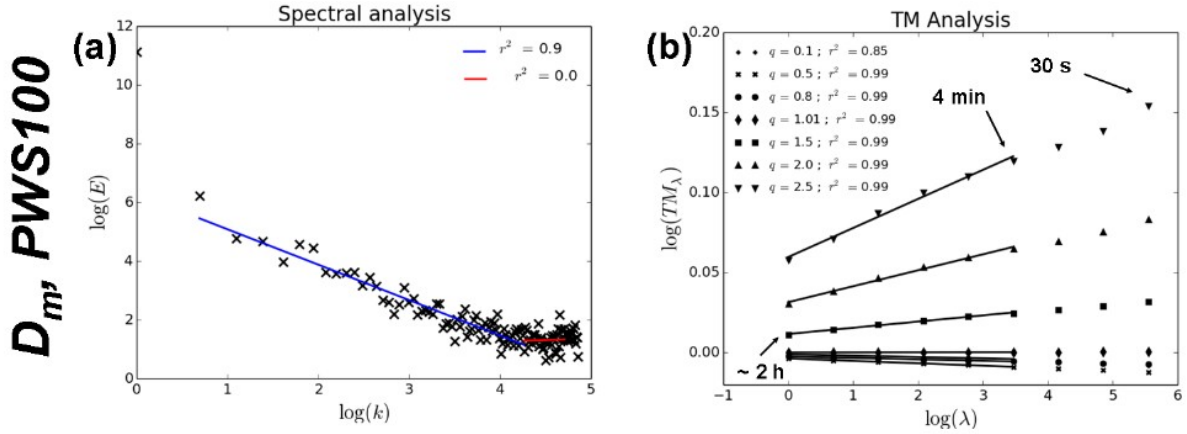

574

575Figure 6: Same as in Fig. 3 but for D_m measured by the PWS100, in (a) a break is considered

576for k=70 (~ 2 min^{-1}), in (b) a break is considered for λ=32 (4 min)

577